

A. K. Plappally

Food Agricultural and Biological Engineering,
The Ohio State University,
Columbus, OH 43210

I. Yakub

PRISM,
Princeton University,
Princeton, NJ 08544;
Mechanical and Aerospace Engineering Department,
Princeton University,
Princeton, NJ 08544

L. C. Brown

Food Agricultural and Biological Engineering,
The Ohio State University,
Columbus, OH 43210

W. O. Soboyejo

Fellow ASME
PRISM,
Princeton University,
Princeton, NJ 08544;
Mechanical and Aerospace Engineering Department,
Princeton University,
Princeton, NJ 08544

A. B. O. Soboyejo

Fellow ASME
Food Agricultural and Biological Engineering,
The Ohio State University,
Columbus, OH 43210

Physical Properties of Porous Clay Ceramic-Ware

The focus of this study is on the physical properties of clay ceramic materials compatible for drinking water filtration. A multiparameter lognormal multivariate regression approach is proposed for assessing the combined effects of quantity of compositional constituent of raw materials used in ceramic manufacture on toughness. The approach was validated for two specimen types (T- and S-specimens) derived from a circular base of the frustum shaped, porous clay ceramic ware (PCCW). The PCCW were manufactured from clay and sieved sawdust mixed at distinct volume fractions. The variation of the porosity and density of the PCCW was studied with respect to the amounts of sawdust and clay used in the manufacturing. The research helped to clearly define the roles of clay and sawdust quantities for strength development in both T- and S-specimen. A generalized experimental approach is proposed for estimation of mechanical properties of clay ceramics as a function of the material constituent fractions. A polynomial relationship was developed between the compressive strength and density of the PCCW material. The statistical model expressions developed herein may be used for the prediction of material and mechanical properties of similar materials, including natural and engineered materials. [DOI: 10.1115/1.4004158]

Keywords: multiparameter modeling, lognormal multivariate regression, clay and sawdust fractions, ceramic strength

1 Introduction

Locally manufactured, low-cost clay ceramics are promising options for drinking water storage and purification [1]. The use of clay ceramic filters for water treatment has impacted the occurrence of water borne diseases across Africa, Asia, and South America [2,3]. There is an abundance of literature documenting the flow behavior through clay ceramic filters, field studies on microbial removal effectiveness, structural damage of filters while in use and during transport, and people/societies satisfaction and health impact of using these ceramic filters [4–10].

Clay and plant by-products, such as sawdust, agricultural residues, husks from rice and coffee, etc., mixed in some composition are used as base materials to manufacture these ceramic devices [5–7]. This mix is moistened, formed, dried and eventually fired to manufacture porous clay ceramic materials, as well as filtration devices. The most commonly used ceramic water filters are frustum-shaped clay ceramics [4].

Fractional changes in composition change the microstructural and mechanical properties [4]. Microstructural flow and mechanical characteristics change geo-spatially due to nonavailability of similar raw material constituents at different locations around the globe [4–8]. Structural porosity and density of porous ceramic materials play a major role in defining their strength [4,9]. Functional challenges, such as water contamination, loading rate, application frequency, material availability, and composition are not the same around the world; hence these parameters also contribute to variability in the physical properties of clay ceramic filters [4,7,10].

From a potter's perspective, physical properties can be affected by manipulating compositions of clay and plant by-products [11,12]. Clay pottery and clay ceramics discussed herein are brittle [4]. Controlled addition of organic or inorganic materials is done to optimize the structural integrity of the clay ceramics and device manufactured from them [10,13]. Strength of the ceramic materials can also be controlled by the influence of firing temperature [8]. Other parameters influencing development of strength are a result of non-uniform forming, such as improper mixing, non-optimal addition of water, uneven drying, etc. [6,14–18]. During transportation ceramic water filters have broken [4,19–22]. Rupture of ceramic water filter has occurred during use [14,15].

In this technical paper, research is focused on providing better understanding of properties, processes and variables responsible for structural integrity of clay ceramic materials used for water filtration. The analysis of strength and other physical properties is complicated by the heterogeneous nature of clay and additive materials, such as sawdust. Following this, a study is undertaken to understand the variability in physical and material properties, such as porosity, density, fracture and compressive strength of clay ceramic materials. The study defines physical properties of these clay ceramics as a function of raw material compositions used in its manufacture. Depending upon the different combinations, a significant variability in physical properties may occur within any clay ceramic material. This suggests that a statistical framework is required for modeling the physical properties of clay ceramic material used for water treatment and storage.

2 Materials and Processing

2.1 Raw Materials. Clay ceramic filter production was initialized by combining specific amounts of natural materials, namely organic material and clay. The organic material was

Contributed by the Materials Division of ASME for publication in the JOURNAL OF ENGINEERING MATERIALS AND TECHNOLOGY. Manuscript received October 2, 2010; final manuscript received April 16, 2011; published online June 24, 2011. Editor: Hussein Zbib.

sawdust containing 80% Oak and 20% Spanish cedar, obtained from a local saw mill [21]. Manual sieving of sawdust whiskers is performed using a 35-1000 mesh (Hamilton Supplies, Hamilton, NJ) to control their dimension. Clay was commercially available from Cedar Heights Redart Air floated Clay, Pittsburgh, PA. The clay ceramic filters developed are called porous clay ceramic ware (PCCW) filters due to their porous structure and base material clay used in its manufacture.

2.2 Manufacturing Process of the PCCW filters. Clay and sawdust were mixed in volume ratios of 75-25, 65-35, and 50-50. Uniform mixing was done with a commercial blender (Model A-200, The Hobart Manufacturing Co., Troy, OH). The blended composite consumed approximately 2 l of water for molding a 6 kg (12lb) dough ball, required to manufacture one porous clay ceramic ware (PCCW) filter. The blended composite was pressed formed to a frustum shape using a hydraulic press (TRD 55002, Torin Jacks, Inc, and Ontario, Canada). The forming process is illustrated in Fig. 1 below. The formed composite at this stage of manufacturing is referred as a greenware [21]. Each of the green wares had an axial length of 26 cm and base diameters of 20 and 23 cm, respectively. They also had a thickness of 0.5 and 1.26 cm on the frustum wall and base, respectively.

Figure 1 shows a two dimensional representation of the step by step axial press forming procedure. The plasticity of clay-sawdust water suspension plays a major role in forming the circular base as well as walls of the frustum shaped green ware. The arrows in Fig. 1 show the direction of transport of the wet clay-sawdust suspension during forming. This plastic flow may align the sieved sawdust fibers along the direction of flow [23]. Rapid changes occur in the microstructures (basically chemical transformation, pore formation or densification) during liquid phase sintering due to the rapid material transport through the fluid [24].

The green wares were kept at room temperature to air dry. The time taken for drying varied from 5–8 days for each of the different constituent, volume ratio mixtures tested here. After air drying, the green wares were oven dried at 100 °C for an hour in order to ensure complete moisture removal. The green wares are subjected to a sequential two step heat treatment. First, the green wares were preheated to approximately 500 °C for 3 h in an electric kiln [18]. The rate of heating was augmented from 50 °C to 100 °C/h, after the kiln had reached 200 °C. The second step was to reheat the green ware in the electric kiln at room temperature to approximately 955 °C. This process was sustained for 5 h at 955 °C after which the furnace was cooled to room temperature [4,21]. The above mentioned procedure of liquid phase sintering helps ceramic compaction and densification [24].

Behavior of manufactured ceramic is controlled by mineral composition, phase change, particle size, environment, and volumetric constituents, particularly decomposable minerals [12]. Sawdust decomposes to charcoal which helps in the production of light weight frustum shaped PCCW. Channel pores are formed within the clay ceramic system as a result of phase transformation or chemical interactions between the constituents namely clay and

sawdust. These porous materials will aid effective water filtration [25].

3 Experimental Procedure

3.1 Material Analysis

3.1.1 Porosity. Porosity measurement for the PCCWs was performed using the mercury intrusion porosimetry (MIP) device (Micromeritics® Autopore III: 9400 digital analyzer). The procedure for using this MIP digital analyzer has been discussed briefly elsewhere [21]. The porosity values varied linearly as a function of the volume fraction of the sawdust used in the ceramic manufacture [4,21]. The relationship is expressed as $\text{Porosity} = a*V + b$, where V is the volume fraction of the sawdust (25%, 35%, and 50%), coefficients a and b are the slope and the intercept, respectively. The coefficient of determination, R^2 , is 99.91% [21]. The pore size distribution within the PCCWs is to be studied and statistically analyzed with respect to the fracture. This discussion is also extended with a brief overview of cumulative pore volume and pore area values, respectively.

3.1.2 Density. A C-S (Volume fraction of clay–Volume fraction of sawdust) notation has been used to describe the specific PCCWs and their corresponding experiments. The densities of the PCCWs (Y_d) were measured using helium pycnometry (Model AccuPyc® 1330 V2. 01, Micromeritics Instrument Corp., Norcross, GA). The samples were ~2-mm diameter particles retrieved from the 75-25, 65-35, 60-40, 50-50, and 85-15 PCCWs, respectively. The variability in densities of the PCCW materials as a function of material composition is to be studied.

3.2 Bending and Compression Experiments

3.2.1 Bending Test. Fracture toughness tests were performed on single-edge notched bend (SENB) specimens with a thickness B of approximately 12.6 mm, width W of approximately 12.6 mm and span S of approximately 75 mm [26,27]. All specimens were uniformly processed with a uniform notch-to-width ratio (α/W) of approximately 0.2519 as shown in Fig. 2, for the SENB tests.

The SENB specimens with notch at center and in a direction parallel to the circumference of the circular ceramic base of the PCCWs are T -specimens as shown in Fig. 4. To evaluate anisotropic mechanical property variations, similar S -specimens with a notch at the center and carved perpendicular to the circumference of the circular ceramic base were prepared as shown in Fig. 3.

The S -specimens are used to study the influence of radial outward plastic flow (Fig. 1) of the clay-sawdust suspension during the axial press forming process of the circular base of the ceramic. The specimen notches were carved out with a low speed diamond saw, and the tests were conducted using a three-point loading apparatus with a span S of approximately 75 mm. For each of the three T -specimen and S -specimen samples, three separate subsamples were taken from each of the 75-25, 65-35, and 50-50 configurations.

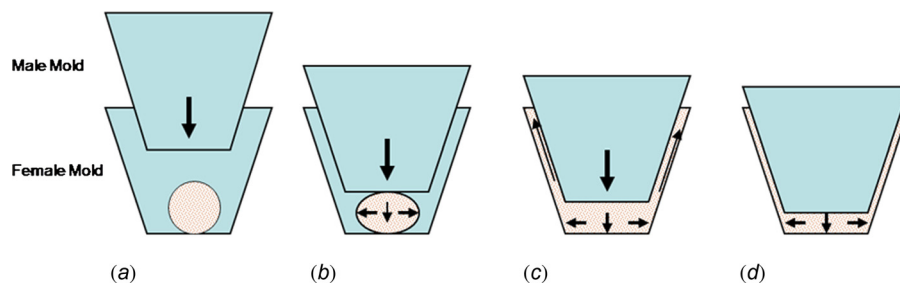


Fig. 1 Two-dimensional representation of development of the frustum-shaped green ware during the axial press forming operation

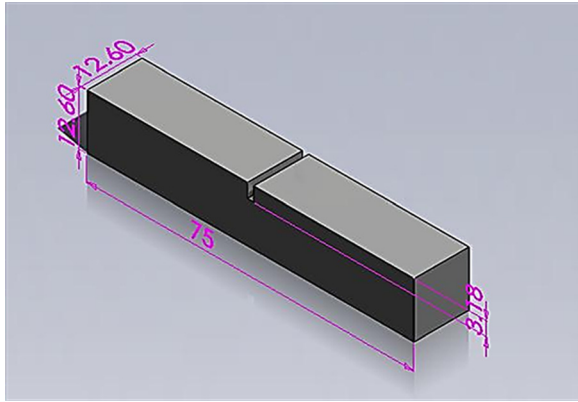


Fig. 2 The three point bend test specimen

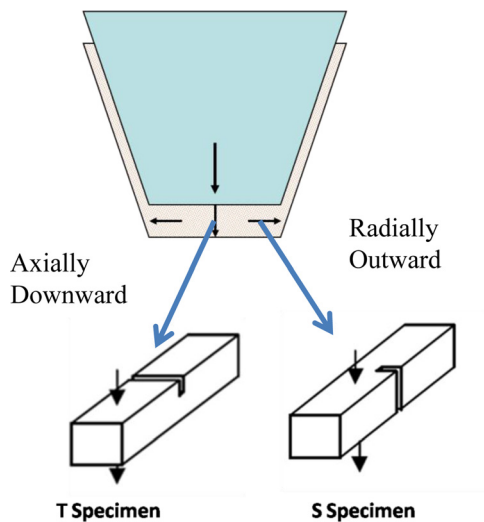


Fig. 3 Characterization of specimens according to the two basic transport modes of wet clay-sawdust suspensions noticed during the axial press forming operation as shown in Fig. 1

An electromechanical microtesting machine (Model 5848, Instron[®], Canton, MA) equipped with a 500-N load cell was used for fracture toughness testing. The tests were performed under load control at a monotonic loading rate of 0.1 N/s (constant loading rate applied on specimens with no reversals from initiation of load application to final fracture as per ASTM E-399-90 Mode I fracture test standard [28,29]). The tests were conducted at a room temperature of 298 K and a relative humidity of 40% to 50%.

Both load and displacement data were recorded digitally using data acquisition software (LabView Version 8.6, NI Inc, Austin, TX). The loads corresponding to specimen failure were used for the calculation of the Mode I fracture toughness, K_{Ic} . Fracture toughness, K_{Ic} , under the linear elastic fracture mechanics is given by [27] as

$$K_{Ic} = f(\alpha/W)(PS/BW^{1.5}) \quad (1)$$

where W and B are the width and thickness of the clay composite ceramic ware (CW) specimen (Fig. 3), respectively, in the direction of the applied load P . Here the geometric and compliance function $f(\alpha/W)$, for a single edge notched specimen is given by [27],

$$f(\alpha/W) = f(\chi) = (3\sqrt{\chi}/2(1+2\chi)((1-\chi)^{1.5})) \times [1.99 - \chi((1-\chi)(2.15 - 3.93\chi + 2.7\chi^2))] \quad (2)$$

3.2.2 Compressive Stress Testing. The compressive strength tests conformed to ASTM 1358 standards. The specimen for the strength tests were cut from the circular base of the frustum shaped PCCWs. Specimens were tested for compressive failure at a sustained static loading rate P of 0.1 N s^{-1} applied parallel to the 35-mm span of the specimens. The tests were carried out on an electro-mechanical machine (Model 8872Instron[®], Canton, MA) with a 10-KN load maximum capacity. The tests were conducted at a room temperature of 298 K and a relative humidity of $\sim 40\%$ to 50%.

4 Statistical Interpretation of Tensile Test Data

The manufacture of multiple PCCW with variable clay to sawdust compositions, production of T and S specimen samples from each of the PCCW and testing them for material properties is time consuming and expensive. Hence, a limited significant number of tensile and compression tests are performed and importance is given to statistical interpretation of the test results. Figure 4 illustrates the tensile test results for the T and S -specimen samples. These tensile (K_{Ic}) test results are independent of crack length, since crack propagation is not considered which might increase the volume of the nonlinear process zone due to micro-cracking [30,31]. Figure 4 plots K_{Ic} data as a function of volume fraction of sawdust.

The K_{Ic} data lies within the range $0.1\text{--}2.0 \text{ Mpa}\cdot\text{m}^{1/2}$ [27,32]. For accepting the plotted K_{Ic} data as material property, a strict criterion is that K_{Ic} data for each specimen tested should be independent of the corresponding specimen thickness, B [27]. This criterion is verified by calculating the Pearsons Correlation Coefficient between K_{Ic} data and corresponding specimen thickness. The value of the Pearsons Correlation Coefficient is -0.0142 at a p -value of 0.915 at 95% confidence level. This confirms that K_{Ic} data in Fig. 4 can be accepted as a material property conforming to plain strain conditions [27].

4.1 Multiparameter Modeling Framework. The influence of different raw material compositions and transport modes (depicted in Fig. 1) on K_{Ic} are not obvious from Fig. 4 [13,30]. To help the potters better understand how different raw material constituents influence pottery strength, a statistical stochastic approach to express K_{Ic} is proposed. The approach will illustrate the lognormal behavior of K_{Ic} , which is clear from the expression in Eq. (1). The approach will model K_{Ic} data as a function of multiple pairs of compositional volumetric data available for clay and sawdust used.

Figure 4 illustrates a nonlinear relationship between K_{Ic} and volume fraction of sawdust. For the sake of simplicity in writing the response variable K_{Ic} is represented by variable “ Y ” from here onwards.

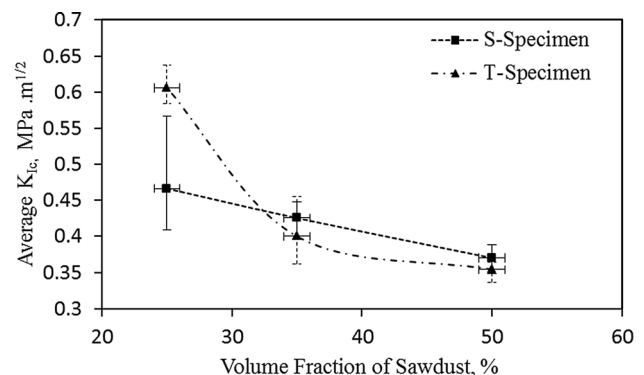


Fig. 4 K_{Ic} versus volume fraction of sawdust percentage, for T and S specimens

It is assumed that Y is a result of superposition of k random predictor variables, X_i , for $i = 1, 2, \dots, k$ with an initial value of Y_0 at time step $t = 0$ (Ref. 33). The variable Y at any step i is a result of an injection of a predictor variable X_i at a previous time step $i-1$, therefore the step i can be expressed as [34]

$$Y_i/Y_{i-1} = X_i^{b_i} \quad \text{for } i = 1, 2, \dots, k \quad (3)$$

where b_i is a constant coefficient for each predictor variable X_i , for $i = 1, 2, \dots, k$. With step by step injection of k multiple predictor variables, the Y value at $i = k$ can be written as

$$Y_k = Y = Y_0 X_1^{b_1} X_2^{b_2} \dots X_k^{b_k} = a \prod_{i=1}^k X_i^{b_i} \quad (4)$$

where Y_0 is the initial value of K_{Ic} . The initial value of Y_0 is represented by an alphabet "a" for simplicity in Eq. (4). Equation (4) can be linearized and rewritten in the form

$$y = y_i = \ln Y = \ln a + \sum_{i=1}^k b_i \ln X_i \quad (5)$$

The value of Y as plotted in Fig. 4 is dimensionally large. So for error reduction in the modeling efforts it is better to use low dimensional response variables. A new response variable is hence defined which must reduce the response variable to a smaller number as well as preserve the properties of Y [35–38]. Hence the new response (quotient) variable is [37,38],

$$G = G_i = X_i/Y_i \quad (6)$$

where X_i is one of the predictor variables, which is supposed to be most important and visible variable in the development of Y (K_{Ic}). From Fig. 4, it is visible that increase in volume fraction of sawdust decreases K_{Ic} irrespective of specimen type.

With this quotient approach, there is an interchange in the roles of the response and predictor variables. This may better explain the major influencing variables and their hierarchy [37,38]. The new response variable G at any time step i may be written as

$$G_i = G_i X_i^{n_i} = m X_i^{n_i} \quad (7)$$

where n_i is constant coefficient of X_i in Eq. (7) for $i = 1, 2, \dots, k$ [36]. Since G would preserve the original trends and properties of Y , the value of G when $i = k$ may be written as [37,38]

$$G_k = G = G_{k-1} X_k^{n_k} = m X_1^{n_1} X_2^{n_2} \dots X_k^{n_k} \quad (8)$$

Similar to development of Eq. (5), linearization of the multiplicative formulation for Eq. (8) is required and is expressed as [39,40]

$$g = g_i = \ln G_i = \ln m + \sum_{i=1}^k n_i \ln X_i = m_0 \sum_{i=1}^k n_i \ln X_i \quad (9)$$

To find the independent influence of each of the predictors X_i for $i = 1, 2, 3, \dots, k$, the following assumptions and procedures are used. Some predictors may be interdependent and would have a correlation coefficient $\rho_{x_i, j}$, where $i = 1, 2, 3, \dots, k$ and $j = 1, 2, 3, \dots, k$.

Mathematically, the interdependent predictor variables $X_{i,j}$ can be converted to independent variables $V_i = \bar{V}_{1,j}$, as prescribed by the steps in the Appendix [4]. In terms of independent predictors V_i , Eq. (8) can be rewritten as:

$$g = e^{m'0} V_1^{\bar{n}_1} V_2^{\bar{n}_2} \dots V_k^{\bar{n}_k} \quad (10)$$

where $m'0, \bar{n}_1, \bar{n}_2, \dots, \bar{n}_k$ are the new model constants of the independent predictor variables in Eq. (10). The procedure pre-

scribed in Appendix is used to convert correlated predictor variables $X_{i,j}$ appearing in Eqs. (8) and (9), to independent predictor variables, V_i .

To accurately model any material property with G , there is a need to determine accurate values of m_0 and other model constants in Eq. (8). To achieve this, the error S of the model should be negligible, such that [40]

$$s = \sum_{i=1}^n \left(g_i - \sum_{d=0}^k n_d x_{di} \right)^2 \quad (11)$$

where $d = 1, 2, 3, \dots, k$. Eq. (11) provides $k+1$ normal equations of the form [34]

$$\partial S / \partial n_d = \sum_{i=1}^n x_{ei} \left(g_i - \sum_{d=0}^k n_d x_{di} \right) = 0 \quad (12)$$

Here the matrix form of Eq. (12) can be rewritten in parts such that $\sum_i x_{di} x_{ei} = n_{de}$ and $\sum_i g_i x_{ei} = G_{d,}$, where $e = 1, 2, 3, \dots, k$ and the $k+1$ normal equations can be written in the form [34]

$$\sum_{d=0}^k n_{de} n_d = G_d \quad (13)$$

By matrix inversion, the value of n_d is calculated as , for $e = 1, 2, 3, \dots, k$. The derived value of n_d minimizes S and improves the prediction of the g model. Mathematical linear regression expressions have been developed to estimate the values of n_d via analysis of empirical K_{Ic} data illustrated in Fig. 4. The expected value of g_i can be expressed as [34]

$$E(g) = m_0 \prod_{i=1}^k E(X_i^{n_i}) \quad (14)$$

The second central moment (Var g) of this distribution may then be expressed as [34]

$$\text{Var } g = \sum_{i=1}^k n_d^2 [\sigma X_i / X_i]^2 G_i^2 \quad (15)$$

The probability distribution function of g_i is expressed as [40,41]:

$$f(g) = \left(1 / g \sqrt{2\pi \text{var } g} \right) \exp \left\{ -0.5 \left(g - E(g) / \sqrt{\text{var } g} \right)^2 \right\}, \quad (16)$$

for $G > 0$

Since the predictor random variables have different magnitudes and dimensions, Eq. (8) can be reformulated as [4]

$$G = G_o \prod_{i=1}^3 (X_i / X_{io})^{n_i} \quad (17)$$

$$a = G_o \left\{ \prod_{i=1}^k X_i^{n_i} \right\}^{-1} \quad (18)$$

where X_{io} for $i = 1, 2, 3, \dots, k$, is the maximum value of X_i for $I = 1, 2, 3, \dots, k$, respectively. This helps in achieving dimensional similarity [4].

5 Results and Discussion

5.1 Material Analysis and Model Prediction

5.1.1 Porosity. Figure 5 depicts a piece-wise constant estimation of pore diameters for the PCCW tested. From Fig. 5, the pore sizes of the clay ceramic ware materials are found to be within 100 to 1 μm .

From Fig. 5, unimodality in pore size distribution is observed in the 50-50 PCCW material, while bimodality is observed in 65-35 and 75-25 specimens. Unimodality in pore sizes is considered

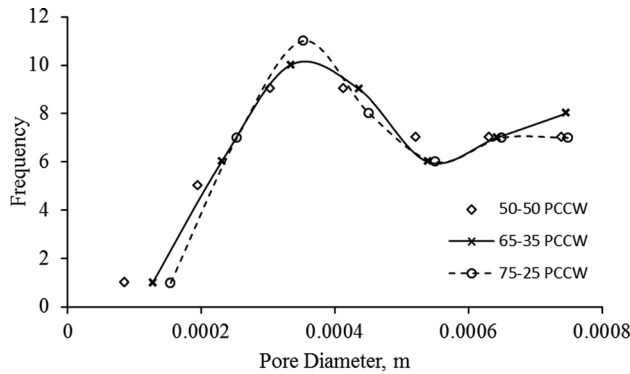


Fig. 5 Pore size distribution in porous clay ceramic ware samples discussed in this study

detrimental to the structural reliability of ceramic materials [42]. A bimodal pore size distribution increases the required energy to cause fractures [42,43]. So, a bimodal pore size distribution in the 65-35 and 75-25 PCCWs also confirms a larger stress intensity factor in comparison to that for the 50-50 PCCW. The cumulative pore volume and pore area of the 50-50 PCCW is 0.3652 ml/g and 1.36 m²/g, respectively. Similarly, the 65-35 and 75-25 PCCWs have cumulative pore volumes of 0.2817 ml/g and 0.2425 ml/g, respectively, and cumulative pore areas of 2.183 m²/g and 1.604 m²/g, respectively. Additional discussion on porosity is in Plapally et al. [29].

5.1.2 Density. The average values of density measurements Y_d (g/cc), for each type of PCCWs are plotted in Fig. 6 as a function of the respective volume fraction of sawdust. The measurements were in agreement with published data and within the range of approximately 2–4 mg/m³ [26,27]. The 60-40 and 85-15 PCCWs were produced following the manufacturing procedure explained earlier using clay and sawdust in volume ratios of 60-40 and 85-15.

The experimental PCCW density data are provided in Table 1 (8 test values per PCCW, to analyze its variation with the corresponding volume fraction of sawdust, X).

The model framework developed for Eq. (8) was applied to these empirical Y_d data in Table 1.

Following the expression in Eq. (9), new model for density prediction is expressed as

$$G = X/Y_d = aX^b \quad (19)$$

$$\ln G = \ln a + b \ln X \quad (20)$$

The regression model in Eq. (19) predicts G as a function of volume fraction of sawdust X with $R^2 = 99.99\%$, and $S = 0.004993$; and may be expressed as

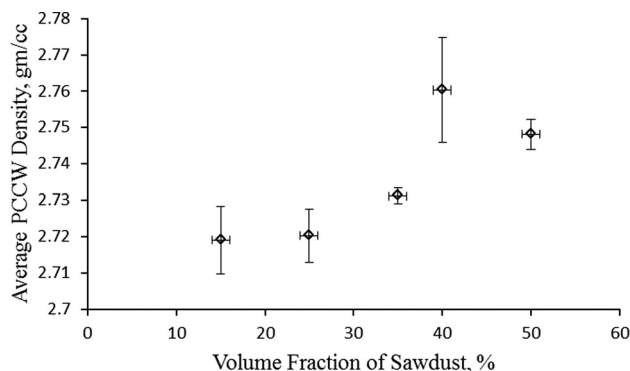


Fig. 6 Average Density (g/cc) as a function of corresponding volume fraction of sawdust used in the PCCWs

Table 1 The density values for the PCCW materials discussed

| PCCWs | Density (g/cc) | | | | | | | |
|-------|----------------|-------|-------|-------|-------|-------|-------|-------|
| | 1 | 2 | 3 | 4 | 5 | 6 | 7 | 8 |
| 85-15 | 2.735 | 2.724 | 2.725 | 2.712 | 2.724 | 2.712 | 2.714 | 2.707 |
| 75-25 | 2.721 | 2.721 | 2.721 | 2.748 | 2.721 | 2.722 | 2.721 | 2.710 |
| 65-35 | 2.734 | 2.730 | 2.729 | 2.730 | 2.732 | 2.733 | 2.728 | 2.728 |
| 60-40 | 2.785 | 2.777 | 2.761 | 2.749 | 2.764 | 2.742 | 2.750 | 2.755 |
| 50-50 | 2.757 | 2.749 | 2.750 | 2.750 | 2.744 | 2.745 | 2.743 | 2.748 |

$$G = e^{-0.978} X^{0.991} \quad (21)$$

Equation (21) can be used to calculate the density of similar clay ceramic material manufactured with any quantity of plant material. From the above discussion on the density and pore areas for the 75-25, 65-35, and 50-50 PCCWs, it can be confirmed that when pores are small, microstructural density is larger [9].

5.2 T-Notch Specimen Toughness and its Prediction as a Function of Raw Material Constituents. From Figs. 4–6, the sawdust variation is found to influence the microstructural properties as well as energy needed to cause fracture. Considering the tensile tests on the T -specimen and following the assumptions outlined while enumerating the multiparameter modeling framework, volume fraction of sawdust is considered as a visible variable while defining G . The predictor variable, X_1 , is the volume of sawdust while X_2 is the volume fraction of clay for the T -specimen tensile test data analysis. For T -specimen, Eq. (6) may be rewritten as $G = X_1/Y$, where Y is K_{Ic} of the T -specimen as illustrated in Fig. 4. Equation may be reformulated as

$$G = mX_1^{n_1} X_2^{n_2} \quad (22)$$

Table 2, shows a step by step improvement in prediction with increasing predictor variables and a decreasing error S of the model. Correlations exist between the predictor variables X_1 and X_2 . At a p -value of <0.005 , the correlation coefficient $[\rho_{x_i, j}]$ between x_1 and x_2 is -0.989 . These correlated predictor variables are transformed to independent entities (V_1 and V_2) using the framework in Appendix. Equation 22 can then be expressed similar to the formulation in Eq. (10) as

$$G = e^{4.38} V_1^{-0.372} V_2^{-1.11} \quad (23)$$

where the magnitude of the coefficients of V_1 confirms that volume fraction of sawdust is the major variable influencing the development of fracture toughness K_{Ic} in T specimens.

The model illustrated in Eq. (23) satisfies [43],

$$\text{Var } g \approx (\bar{n}_1)^2 \text{Var}(V_1) + (\bar{n}_2)^2 \text{Var}(V_2). \quad (24)$$

where $\text{Var } g = 0.293 \approx (-0.372)^2 1.989 + (-1.11)^2 0.0114$; and thus $0.293 \approx 0.289$. The mathematical verification of Eq. (23) also

Table 2 Summary of change in model constants, coefficient of determination R^2 and error value S , with injection of predictor variables X_1 and X_2 for Eq. (22)

| Predictor variables \ model coefficients | m_0 | n_1 | n_2 | R^2 | S |
|--|-------|-------|-------|-------|-------|
| X_1 | -1.92 | 1.77 | — | 96.3 | 0.111 |
| X_2 | -20.3 | 3.5 | 2.95 | 98.4 | 0.078 |

confirms the major influence of volume fraction of sawdust on the K_{Ic} of the T -specimen.

Figure 7 plots empirical K_{Ic} for T specimen calculated (using Eq. (1)) as a function of predicted K_{Ic} for T specimen calculated by the multiparameter model in Eq. (22). Table 3 illustrates the different models tests performed on the fracture toughness data of the T -specimen. Table 3 confirms the better determination characteristics of the lognormal G model.

Theoretical models for K_{Ic} of T notch specimen as proposed in Eq. (22) following the framework in Eq. (8) and experimental cumulative frequency is found to have a maximum discrepancy $D_n = 0.212$. The maximum discrepancy D_n is found to be less than critical maximum difference $D_n^{0.5} = 0.262$ [40]. Therefore the model proposed in Eq. (22) is more appropriate at a 5% significance level for T -notch toughness as illustrated in Table 4 below.

5.3 S-Notch Specimen Strength and its Prediction as a Function of Raw Material Constituents. From Fig. 4, the resistance to crack for T and S specimens is found to vary as follows

$$K_{Ic\ 75-25-T} > K_{Ic\ 75-25-S}, K_{Ic\ 65-35-T} < K_{Ic\ 65-35-S} \text{ and } K_{Ic\ 50-50-T} < K_{Ic\ 50-50-S}.$$

There will be a specific percentage above 25% volume fraction of sawdust beyond which fracture toughness of T specimen is reduced in comparison to the S specimen. This variation in toughness indicates the impact of different modes of transport in the development of the ceramic base as illustrated in Fig. 1. The predictor variable X_1 , is the volume of sawdust while X_2 is the volume fraction of clay for the S -specimen tensile test data analysis. The quotient response variable G may be written as $G = X_1/Y$, where Y is the K_{Ic} of the S -specimens as illustrated in Fig. 4. For the S -specimen Eq. (8) can be reformulated as

$$G = mX_1^{n_1}X_2^{n_2} \quad (25)$$

where X_2 is the volume fraction of clay and m, n_1, n_2 represent the model constants for the regression equation. The model constants for Eq. (25) are tabulated in Table 5.

Table 5, shows the step by step improvement in prediction with increasing predictor variables and a decreasing error S of the model. The correlation coefficient between the predictor variables X_1 and X_2 [ρ_{X_i, X_j}] is -0.989 at p value less than 0.005. These correlated predictor variables are transformed to independent entities (V_1 and V_2) using Eq. (10). Equation (25) can then be rewritten with independent predictor variables similar to the formulation in Eq. (10) as

$$G = e^{4.44}V_1^{-0.281}V_2^{-0.161} \quad (26)$$

where the magnitude of the coefficient of V_2 confirms that volume fraction of clay is the major variable influencing the development of fracture toughness for S specimens. The coefficient of determi-

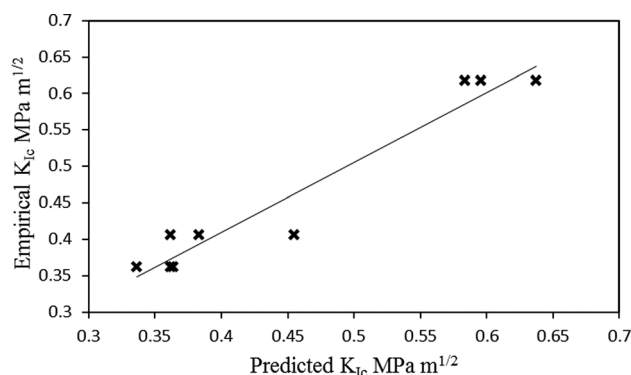


Fig. 7 Fit between K_{Ic} predicted using Eq. (22) and K_{Ic} measured for T specimen

Table 3 Results of different distributions tested towards fitting experimental K_{Ic} data for T -specimens

| Model | Response variables | R^2 | S |
|-----------|--------------------|-------|--------|
| Normal | Y | 0.75 | 0.06 |
| Lognormal | y | 0.929 | 0.0782 |
| Normal | G | 0.974 | 7.509 |
| Lognormal | g | 0.984 | 0.0782 |

Table 4 D_n and $D_n^{0.5}$ of Kolmogorov Smirnov Test for evaluating K_{Ic} prediction models for T specimen

| Kolmogorov Smirnov Test at 5% Level of confidence | | | |
|---|-------|---------------------|---------|
| | g | No. of Data Samples | p-value |
| D_n | 0.212 | 27 | <0.010 |
| Critical value of [40] | 0.262 | 27 | |

Table 5 Summary of change in model constants, coefficient of determination R^2 and error value S , with injection of predictor variables X_1 and X_2 for Eq. (25)

| Predictor variables \ model coefficients | m_0 | N_1 | n_2 | R^2 | S |
|--|--------|-------|-------|-------|-------|
| X_1 | -0.267 | 1.32 | | 94.1 | 0.116 |
| X_2 | 2.69 | 1.04 | -0.48 | 94.2 | 0.113 |

nation R^2 and error S for the model in Eq. (26) is same as elaborated in Table 5.

It is also seen that the model illustrated in Eq. (26) satisfies [44]

$$\text{Var } g \approx (\bar{n}_1)^2 \text{Var}(V_1) + (\bar{n}_2)^2 \text{Var}(V_2). \quad (27)$$

where $\text{var } g = 0.167 \approx (-0.281)^2 1.989 + (-0.161)^2 0.0114$ and thus $0.167 \approx 0.157295$. The above results for Eq. (26), also inform that the volume fraction of clay is the major influence to fracture toughness K_{Ic} for S specimen. Figure 8 plots empirical K_{Ic} for S specimen calculated (using Eq. (1)) as a function of predicted K_{Ic} for S specimen calculated by the multiparameter model in Eq. (25). In comparison to the model for T notch, Eq. (22), the model for S notch, Eq. (25) is not a very good predictor of toughness for S -specimens.

Table 6 illustrated the coefficient of determination R^2 and standard error of the model S for different models tested on the experimental data of S -specimen plotted in Fig. 4.

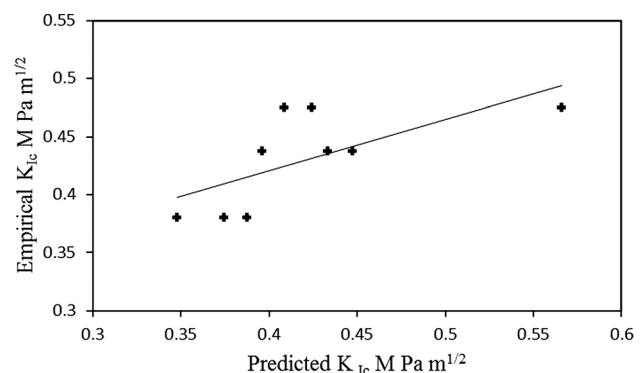


Fig. 8 Plot between K_{Ic} measured for S specimen versus K_{Ic} predicted using Eq. (25)

Table 6 Results of different distributions tested towards fitting experimental K_{Ic} data for S-specimens

| Model | Response variables | R^2 | S |
|-----------|--------------------|--------|------|
| Normal | Y | 0.448 | 0.48 |
| Lognormal | y | 0.4933 | 0.11 |
| Normal | G | 0.90 | 7.3 |
| Lognormal | g | 0.942 | 0.11 |

Theoretical models for K_{Ic} of S specimens as proposed in Eq. (25) following the framework in Eq. (8) and experimental cumulative frequency is found to have a maximum discrepancy $D_n = 0.174$. The maximum discrepancy D_n is found to be less than critical maximum difference $D_n^{0.5} = 0.262$ [40]. Therefore the model proposed in Eq. (25) is found to be more appropriate at a 5% significance level as illustrated in Table 7 below.

5.4 Application of Proposed Models to Data. To further validate the proposed models in Eqs. (8), (23), and (25), they were applied to the data of Monteiro et al. [44]. These data are from clay ceramics containing coal fly ash as the additive instead of sawdust. Figure 9 illustrates the variation of fracture toughness, Y_{fac} , as a function of percentage by weight of fly ash, X_{fac1} , and clay, X_{fac2} . Monteiro et al. measured fracture toughness using non-destructive testing methods and did not follow procedures of ASTM E-399 code for Mode I fracture [44,45].

Subsequent to the assumptions outlined while enumerating the multiparameter framework in Eq. (6), the response quotient variable is expressed as $G = G_{fac} \rightarrow X_{fac1}/Y_{fac}$. Similar to Eqs.23 and 25, the model for fracture toughness of clay ceramics containing coal fly ash can now be expressed as

$$G = G_{fac} = mX_{fac1}^{n1} X_{fac2}^{n2} \quad (28)$$

The correlation coefficient between the predictor variables X_1 and X_2 [$\rho_{fac1,j}$] is -0.894 at p -value ≤ 0.001 . The coefficient value of -0.894 is close to that of the clay and sawdust values from earlier. The multivariate regression expression is derived by following the framework in Appendix and Eq. (10) can be rewritten as

$$G_{fac} = e^{-2.26V_{fac1}^{-1.26}V_{fac2}^{-1.24}} \quad (29)$$

where V_{fac1} and V_{fac2} are the independent predictor variables obtained after removing the interdependence between X_{fac1} and X_{fac2} . The validation lognormal model in Eq. (28) predicts fracture toughness with an $R^2 = 99.9\%$ and $S = 0.0554$. The formulation in Eq. (9) is a model which promises a better prediction of fracture toughness in similar systems.

6 Compressive Strength Analysis and Model Prediction

Production of the clay ceramics from heterogeneous natural materials i.e., clay and sawdust, was achieved by procedures including compressive forming, sintering etc. Therefore there exist high probabilities of existence of inhomogeneity on the sur-

Table 7 D_n and of Kolmogorov Smirnov Test for evaluating K_{Ic} prediction models for S- specimen

| Kolmogorov Smirnov test at 5% significance level | | | |
|--|-------------------|----------------|---------|
| | g (from Eq. (25)) | No. of Samples | p-value |
| D_n | 0.174 | 27 | 0.042 |
| Critical value of [40] | 0.262 | 27 | |

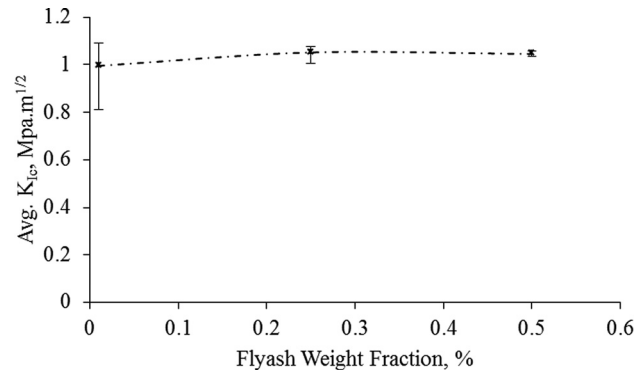


Fig. 9 Fracture toughness (Y_{fac}) in clay ceramics containing fly ash as a function of its manufacturing component X_{fac1} ([44])

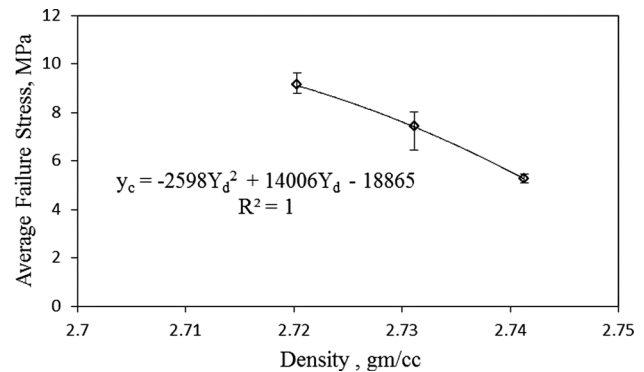


Fig. 10 The average failure stress as a function of density of the 75-25, 65-35, and 50-50 PCCW material

face of the clay ceramic. This inhomogeneity may become an initiator of structural breakdown under some applied force [9]. The applied force should overcome the particle–particle interaction energy determined by Vander Waals forces between the particles within such heterogeneous porous systems, such as PCCW [9]. There is a heavy dependence of failure loads on the density of the heterogeneous porous materials [9]. Compressive load tests conforming to ASTM C1358 were performed on 75-25, 65-35, 50-50 PCCW specimens [46]. The test results plotted in Fig. 10 confirm decrease in compressive load supporting capacity with increase in average density, Y_d , of the PCCWs.

A polynomial relationship exists between failure strength and structural density of the porous heterogeneous materials [9], as illustrated in Fig. 10, where the variable Y_c denotes the average compressive failure stress and the variable Y_d denotes the density of the PCCW material.

7 Conclusions

The conclusions from the experimental data and theoretical analysis of the porous clay ceramic ware physical properties are summarized below,

1. From the study on pore size distributions, the 50-50 PCCW is found to be structurally less reliable than 65-35 and 75-25 PCCW materials.
2. A simple model is proposed to predict density of the porous clay ceramic ware as a function of volume fraction of sawdust.
3. A multiparameter lognormal multivariate regression approach is proposed for assessing the combined effects of quantity of compositional constituent of raw materials on the toughness of the porous clay ceramic ware material. The approach has been validated for two specimen types derived from a circular base of the frustum shaped ceramic ware.

The approach helped to clearly define the roles of clay and sawdust quantities for strength development in both *T*- and *S*-specimen.

4. The comparative study of toughness characteristics of the *T*- and *S*-specimen illustrates the possible influence of the transport of the moist clay-sawdust suspension on the final strength of the clay ceramic.
5. Resistance to compressive forces decreases with increase in material density for clay ceramics.
6. A polynomial relationship between compressive strength and density of the corresponding ceramic is proposed.

Acknowledgment

This work is a part of the study conducted under the research partnership of Princeton University and The Ohio State University. This research partnership was supported by the Division of Materials Research, National Science Foundation (DMR 0231418), USA and The Grand Challenges Program at Princeton University. The authors also acknowledge the support provided by the Ceramic Arts Department, Department of Mechanical and Aerospace Engineering and Princeton Institute for Science and Technology, PRISM, at Princeton University, NJ, for providing access to laboratories for conducting material processing and analysis. The authors also thank the Food, Agricultural and Biological Engineering Department, The Ohio State University, Columbus, OH for their support throughout the work.

Nomenclature

- a = model coefficient
- b = model coefficient
- B = thickness of the SENB specimen
- d = subscript
- e = subscript
- E = expected value
- fac = fly ash clay (Subscript)
- G = assumed variable in the form of quotient X/Y
- g = natural logarithm of G
- i = subscript
- I = identity matrix
- n_1, n_2 = model constants
- n_{de} = invertible matrix
- \bar{n}_2 = model constant for the independent variables
- m_0 = model coefficient
- P = applied load in N
- S = span or length of the SENB specimen
- \bar{T} = transformation matrix

- V_1, V_2 = independent predictor variables after removing interdependence between X_1 and X_2
- W = width of the SENB specimen
- X_1, X_2 = assumed variable predictors
- X_{fac1} = weight fraction of fly ash
- X_{fac2} = weight fraction of clay
- x = natural logarithm of X
- Y = assumed variable denoting response variable
- Y_d = density of the PCCW material
- Y_{fac} = fracture toughness of clay ceramic containing coal fly ash
- y = natural logarithm of Y
- y_c = average compressive failure stress for PCCW material

Greek Symbols

- α = three point bend pre crack or notch size
- ρ = correlation coefficient
- σ = standard deviation of Lognormal model
- μ = mean value
- θ = eigen space
- π = 3.14
- Φ = normalized eigen vector
- χ = variable (α/W)
- λ = eigen value

Appendix

$[\rho x_{i,j}]$ is a square matrix, $k \times k$, and if $[\theta_{i,j}]$ is a vector in the null space of $[\rho x_{i,j}]$ and exist in the n dimensional space of the predictor variable $X_{i,j}$ data set, then [4]

$$[\rho x_{i,j}] [\theta_{i,j}] = \lambda_{i,j} [I] [\theta_{i,j}] \quad (A1)$$

$$[\lambda_{i,j} [I] - [\rho x_{i,j}]] [\theta_{i,j}] = 0 \quad (A2)$$

Here $[\theta_{i,j}]$ is the null space of the characteristic equation term and left hand also represents two orthogonal vectors in the inner product space. It should be noted that $[\theta_{i,j}]$ contains all vectors perpendicular to the column spaces containing all the predictor variables. There will be one eigen space $[\theta_{i,j}]$ for each distinct eigenvalue $[\lambda_{i,j}]$ for $i = 1, 2, \dots, n$ and $j = 1, 2, \dots, k$ when $n > k$ and so there will be k eigen spaces for . Trace of the eigen value matrix also defines the total variance of the predictor variables [4].

$[\bar{T}]$ is an orthogonal square matrix of size, $k \times k$, with normalized eigen vectors $[\theta_{i,j}]$ for the three participating predictor variables. The normalized eigen vectors can be represented as [4]

$$[\phi] = \begin{bmatrix} (\theta_1^1)^2 / ((\theta_1^1)^2 + \dots + (\theta_k^1)^2) & \dots & (\theta_1^k)^2 / ((\theta_1^1)^2 + \dots + (\theta_k^1)^2) \\ \vdots & \ddots & \vdots \\ (\theta_k^1)^2 / ((\theta_1^1)^2 + \dots + (\theta_k^1)^2) & \dots & (\theta_k^k)^2 / ((\theta_1^1)^2 + \dots + (\theta_k^k)^2) \end{bmatrix}^{1/2}$$

Then $[\bar{T}] = [\phi]^t$, which constitutes the transformation matrix $[\bar{T}]$. The correlated predictor matrix column elements $X_i = \bar{X}_{i,j}$ for $i = 1, 2, \dots, k$ with correlation coefficient are linearly transformed into mathematically uncorrelated variables $V_i = \bar{V}_{i,j}$ and scaled as [4]

$$\frac{(\bar{X}_{i,j} - \mu_{\bar{X}_{i,j}})}{\sigma_{\bar{X}_{i,j}}} = [\bar{T}] \left[\frac{[V_{i,j}]}{\sqrt{\lambda_{i,j}}} \right] \quad (A3)$$

The left hand side of the above equation are standard normal variates of the predictor variables $X_{i,j}$ for $i \neq j$ and $i = 1, 2, 3$ having zero mean and unit standard deviation. Here $\mu_{\bar{X}_{i,j}}$ and $\sigma_{\bar{X}_{i,j}}$ are the parameters of a normal distribution. The $V_{i,j}$ for $i = 1, 2, 3$ in Eq. (13), are the independent normal predictor variables with $\lambda_{i,j}$ for $i = 1, 2, 3$ the corresponding variances [4].

References

- [1] Brown, J., and Sobsey, M. D., 2010, "Microbiological effectiveness of locally Produced Ceramic Filters for Drinking Water Treatment in Cambodia," *J. Water Health*, 8(1), pp. 1–10.

- [2] Du Preez, M., Conroy, R. M., Wright, J. A., Moyo, S., Potgieter, N., Gundry, S. W., 2008, "Use of Ceramic Water Filtration in the Prevention of Diarrheal Disease: A Randomized Controlled Trial in Rural South Africa and Zimbabwe," *Am. J. Trop. Med. Hyg.*, **79**(5), pp. 696–701.
- [3] Plappally, A., Chen, H., Ayinde, W., Alayande, S., Usoro, A., Friedman, K., Dare, E., Ogunyale, T., Yakub, I., Leftwich, M., Malatesta, K., Rivera, R., Brown, L., Soboyejo, A. and Soboyejo, W., 2011, "A Field Study on the Use of Clay Ceramic Water Filters and Influences on the General Health in Nigeria," *J. Health Hum. Behav.*, **1**(1), pp. 1–22. (22 Feb 2011) Available online at: (<http://www.asciencejournal.net/asi/index.php/HBPH/article/view/109>). Date accessed: 19 Mar. 2011.)
- [4] Plappally, A. K., 2010, "Theoretical and Empirical Modeling of Flow, Strength, Leaching and Micro-Structural Characteristics of V Shaped Porous Ceramic Water Filters," Doctoral Dissertation, Publication No. 3428662, The Ohio State University, Columbus, OH.
- [5] Hwang, R. E. Y., 2003, "Six-Month Field Monitoring of Point-Of-Use Ceramic Water Filter by Using H₂S Chapter Strip Most Probable Number Method in San Francisco Libre, Nicaragua," Masters of Engineering thesis, MIT, Department of Civil and Environmental Engineering, Cambridge, MA.
- [6] Klarman, M., 2009, "Investigation of Ceramic Pot Filter Design Variables," Master's thesis, Rollins School of Public Health, Emory University, Atlanta, GA.
- [7] Oyanedel-Craver, A. V., and Smith, J. A., 2008, "Sustainable Colloidal Silver Impregnated Ceramic Filter for Point of Use Water Treatment," *Environ. Sci. Technol.*, **42**(3), pp. 927–933.
- [8] Nandi, B. K., Uppaluri, R., and Purkait, M. K., 2008, "Preparation and Characterization of Low Cost Ceramic Membranes for Micro-Filtration Application," *Appl. Clay Sci.*, **42**(1–2), pp. 102–110.
- [9] Gladkov, S. O., 2003, *Dielectric Properties of Porous Media*, Springer-Verlag, New York.
- [10] Lantagne, D., Klarman, M., Mayer, A., Preston, A., Napotnik, J., and Jellison, K., 2010, "Effect of Production Variables on Microbiological Removal in Locally-produced Ceramic Filters for Household Water Treatment," *Int. J. Environ. Health Resour.*, **20**(3), pp. 171–187.
- [11] Davidge, R. W., 1979, *Mechanical Behavior of Ceramics*, 1st ed., The Syndics of the Cambridge University, New York.
- [12] Henry, E. C., 1955, "Clay Technology in Ceramics," Proceedings of Clays and Clay Technology, First National Conference on Clays and Clay technology, Bulletin 169, San Francisco, CA.
- [13] Papargyris, S. A., Cooke, R. D., Papargyris, D. A., Botis, A., Papaploymrou, G., and Papargyris, A. D., 2003, "Mechanical Properties of Short Oxide Fibres-Kaolin Clay Matrix Composite," *Br. Ceram. Trans.*, **102**(5), pp. 193–203.
- [14] Brown, J., and Sobsey, M., 2006, "Independent Appraisal of Ceramic Water Filtration Interventions in Cambodia," Final report, University of North Carolina of Public Health, Department of Environmental Sciences and Engineering, Submitted to UNICEF.
- [15] Roberts, M., 2004, "Field Test of a Silver-Impregnated Ceramic Water Filter, Vientiane, Lao PDR: 30th WEDC International Conference." Available online at <http://wedc.lboro.ac.uk/conferences/pdfs/30/Roberts.pdf>.
- [16] Sobsey, M., and Brown, J., 2006, "Post Project Appraisal of Large-scale HWTS: Lessons from Cambodia, 2002–2006," IWA Beijing Conference, WHO Household. Available online at (http://www.iwahq.org/uploads/conference_graphics/beijing2006/workshops/who%20household/Mark%20Sobsey%20&%20Joe%20Brown.pdf).
- [17] Hagan, J., Harley, N., Pointin, D., Sampson, M., Vanna S., and Smith, K., 2009, *Ceramic Water Filter Handbook*, Resource Development International, Cambodia.
- [18] Cuff, Y. H., 1996, *Ceramic Technology for Potters and Sculptors*, University of Pennsylvania, Philadelphia.
- [19] CAWST, 2009, Water Hygiene and Sanitation, January 2009, CAWST available online (<http://www.cawst.org/en/resources/pubs/file/59-south-asia-low-eng>) accessed June 2009.
- [20] Murcott, S., Soboyejo, W. O., Yakub, I., and Plappally, A. K., 2008, private Communication.
- [21] Plappally, A. K., Yakub, I., Brown, L. C., Soboyejo, W. O., and Soboyejo, A. B. O., 2009, "Theoretical and Experimental Investigation of Water Flow through Porous Ceramic Clay Composite Water Filter," *Fluid Dyn. Mater. Process.*, **5**(4), pp. 373–398.
- [22] Waters, T., 2010, "The Effect of Compositional and Geometrical Changes to the Bending Strength of the Ghanaian Ceramic Pot Filter", Masters of Engineering thesis, MIT, Department of Civil and Environmental Engineering, Cambridge, MA.
- [23] Papargyris, S., Tsipas, D., Botis, A., Spiliotis, X., and Papargyris, A., 2006, "Characterisation of Carbon Fibre Kaolin Matrix Composites," *Adv. Sci. Technol.*, **45**, pp. 1450–1455.
- [24] Kang, L. S.-J., 2005, *Sintering: Densification, Grain Growth and Microstructure*, Elsevier Butterworth-Heinemann, Burlington, MA.
- [25] Mosin, Y., Vorob'eva, V. V., Kostin, S. V., and Pristokokov, V. A., 1996, Penetrable Ceramic Materials Based on Clays with a Controllable Porous Structure, *Ogneup. Tekh. Keram.*, **4**, pp. 14–17.
- [26] Ashby, M. F., 1999, *Materials Selection in Mechanical Design*, 2nd ed., Oxford, Butterworth–Heinemann.
- [27] Soboyejo, W., 2003, *Mechanical Properties of Engineered Materials*, Marcel Dekker, New York.
- [28] Savastano, H., Turner, A., and Mercer, C., 2006, "Mechanical Behavior of Cement-based Reinforced with Sisal fibers," *J. Mater. Sci.*, **41**, pp. 6938–6948.
- [29] Suresh, S., 1991, *Fatigue in Materials*, Cambridge University, New York.
- [30] Buresch, F. E., 1985, "Relation Between the Damage in and Microstructure of Ceramics," *Mater Sci Eng.*, **21**, pp. 187–194.
- [31] Mecholsky, J. J., Freimam, S. W., and Rice, R. W., 1976, "Fracture Surface Analysis of Ceramics," *J. Mater. Sci.*, **11**(7), pp. 1310–1319.
- [32] Wegst, U. G. K., and Ashby, M. F., 2004, The Mechanical Efficiency of Natural Materials, *Philos. Mag.*, **84**(21), pp. 2167–2186.
- [33] Hauge, M., and Thaulow, C., 1993, Statistical Evaluation of Fracture Toughness Test Data, *Fatigue Fract. Eng. Mater. Struct.*, **16**(11), pp. 1187–1202.
- [34] Benjamin, J. R., and Cornell, A. C., 1970, *Probability, Statistics, and Decisions for Civil Engineers*, McGraw Hill, New York.
- [35] Tabuada, P., and Pappas G.J., 2005, "Quotients of Fully Non Linear Control Systems," *SIAM J. Sci. Comput. (USA)*, **43**(5), pp. 1844–1866.
- [36] Bulmer, M. G., 1979, *Principles in Statistics*, Dover Publication Inc., Mineola, NY.
- [37] Sussman, H., 1997, "Existence and Uniqueness of Minimal Realizations of Nonlinear Systems," *Math. Syst. Theory*, **10**, pp. 263–284.
- [38] Pappas G. J., and Simic, S., 2002, "Consistent Hierarchies of Affine Nonlinear Systems," *IEEE Trans. Autom. Control*, **47**(5), pp. 745–756.
- [39] Soboyejo, A. B. O., 1965, "Plastic Flow in Concrete," Technical Report No. 52, Department of Civil Engineering, Stanford University, Stanford, CA.
- [40] Ang, A.H.-S. and Tang, W. H., 1984, *Probability Concepts in Engineering Planning and Design. Volume II—Decision, Risk, and Reliability*, John Wiley and Sons, New York.
- [41] Haldhar, A., and Mahadevan, S., 2000, *Probability, Reliability and Statistical Methods in Engineering Design*, John Wiley and Sons, New York.
- [42] Brito, M. E., 2007, Developments in Porous, Biological and Geopolymer Ceramics: Ceramic Engineering and Science Proceedings (The American Ceramic Society's 31st International Conference on Advanced Ceramics and Composites, held in Daytona Beach, Florida, January 21–26, 2007), Vol.28(9), John Wiley Publishers, NY.
- [43] Soboyejo, A. B. O., 1968, "Propagation of Errors and Tolerance Analysis in Engineering Design and Stress Analysis Problems," Recent Advances in Stress Analysis: New Concepts and Techniques and their Practical Application, The Joint British Committee for Stress Analysis March 26–29th 1968.
- [44] Monteiro, R. C. C., Lima, M. M.R. A., and Alves, S., 2008, "Mechanical Characteristics of Clay Structural Ceramics Containing Coal Fly Ash," *Int J Mech Mater Des.*, **4**(2), pp. 213–220.
- [45] American Society for Testing and Materials, 1997. Standard Test method for plane strain fracture toughness of metallic materials E399, ASTM, West Conshohocken, Book of Standards Vol. 03.01, pp. 31.
- [46] American Society for Testing and Materials, 1998. Standard Test method for monotonic compressive strength testing of continuous fiber reinforced advanced ceramics with rectangular cross section of test specimens at ambient temperatures, C1358-05, C 28.07 subcommittee, ASTM, West Conshohocken, Book of Standards Vol. 15.01, pp. 12.